(Preprint) AAS 25-529

USING MOTION PRIMITIVES TO GENERATE INITIAL GUESSES FOR TRAJECTORIES TO SUN-EARTH L2

Natasha Bosanac*

This paper focuses on generating initial guesses for a spacecraft trajectory from an Earth-Moon L1 Lyapunov orbit to a Sun-Earth L2 Lyapunov orbit. To achieve this goal, a motion primitive approach to trajectory design is employed. Motion primitives are generated as fundamental building blocks of motion in each of the Earth-Moon and Sun-Earth circular restricted three-body problems. Sequences of these primitives are then generated by searching a motion primitive graph that captures their sequential composability within and between dynamical models. These sequences are processed to extract initial guesses for a transfer.

INTRODUCTION

Robotic servicing has the potential to increase the sustainability of space operations well beyond low Earth orbit. Mission concept development for prior and future large observatories operating in orbits around Sun-Earth L2 have included discussions of the architecture and technologies required to render robotic servicing feasible [1–3]. In making this determination, key considerations that impact the trajectory of a robotic servicer spacecraft include, but are not limited to, 1) the holding location of a servicer spacecraft before transferring to the location of an observatory, 2) whether the observatory is serviced near Sun-Earth L2, 3) the response time and maneuver requirements for the servicer spacecraft, and 4) whether a servicer could be reused, refueled, and/or transfer hardware components at a depot located in the Earth-Moon system. These outstanding questions benefit from analysis of the associated trajectory tradespace for a robotic servicer.

A wide variety of researchers within our community have used dynamical systems theory to study segments of the tradespace of trajectories between cislunar space and orbits near Sun-Earth L1 or L2. For instance, Farquhar, Muhonen, and Church presented complex trajectories for the International Sun-Earth Explorer 3 (ISEE-3) spacecraft from a Sun-Earth L1 orbit to the Earth's geomagnetic tail [4]. Howell, Barden, and Lo generated multiple transfers from the Earth vicinity to Sun-Earth libration point orbits and between them [5]. Folta and Webster generated transfers for a robotic servicer from Earth-Moon L2 halo orbits and distant retrograde orbits to Sun-Earth L2 [6]. Similarly, Ojeda Romero and Howell generated geometrically diverse transfers with impulsive maneuvers from a geosynchronous transfer orbits to periodic and quasi-periodic orbits near Sun-Earth L1 and L2 [7]. Pascarella et al. have also generated various trajectories with impulsive and continuous thrust maneuvers from an Earth-centered orbit to Sun-Earth L2 [8]. These papers, and many more within the astrodynamics community, motivate continued development of procedures for generating complex trajectories across a diverse tradespace.

*Associate Professor, Colorado Center for Astrodynamics Research, Smead Department of Aerospace Engineering Sciences, University of Colorado Boulder, 3775 Discovery Drive, Boulder, CO 80303.

Recently, Smith and Bosanac introduced a motion primitive approach to trajectory design that was inspired by their use in robotics [9, 10]. Motion primitives have been defined throughout the literature as fundamental building blocks of motion [11]. As a result, sequences of these primitives have supported constructing complex paths. Smith and Bosanac adapted this idea to define a motion primitive for spacecraft trajectories as an arc that summarizes the geometry of nearby arcs and supplies a building block for the trajectory design process [9, 10]. Expanding upon their use in path-planning, Smith and Bosanac then constructed a motion primitive graph to generate initial guesses from sequences of these primitives in the Earth-Moon system [10]. Through their initial proof of concept, they demonstrated that motion primitives have the potential to support 1) rapid and automated trajectory design and 2) efficient exploration of the trajectory trade space. Since this first proof of concept, Miceli and Bosanac have substantially built upon this procedure to improve the automation of the approach as well as the quality and diversity of the resulting initial guesses; this updated procedure is used as a foundation for this paper [12]. In addition, Gillespie, Miceli, and Bosanac have extended this idea to construct behavioral motion primitives that summarize natural and controlled arcs with a similar geometry while also encoding the associated maneuvering behaviors [13]. The improved procedure for generating the motion primitives, as presented in both of these papers, is used here.

This paper leverages a motion primitive approach to construct initial guesses for a planar spacecraft trajectory from an Earth-Moon L_1 Lyapunov orbit to a Sun-Earth L_2 Lyapunov orbit. To support preliminary exploration of the solution space, motion primitives for natural trajectories are independently constructed to summarize arcs along stable and unstable manifolds of L_1 and L_2 Lyapunov orbits in each of the Earth-Moon and Sun-Earth circular restricted three-body problems (CR3BP). The sequential composability of each pair of primitives is then assessed to construct a motion primitive graph. In this graph, primitives that are closely located within the configuration space are connected in two cases: if they are generated in the same CR3BP, or if a primitive from the Earth-Moon CR3BP passes close to a primitive from the Sun-Earth CR3BP at a sufficient distance from the Earth. This graph is then searched to generate a sequence of primitives, from both dynamical models, that predicts the existence of a nearby continuous trajectory with impulsive maneuvers. Furthermore, distinct motion primitive sequences are used to generate geometrically distinct initial guesses. This approach is demonstrated by generating initial guesses for planar transfers, assuming the Earth-Moon and Sun-Earth orbit planes coincide.

BACKGROUND

Circular Restricted Three-Body Problem

The motion of a spacecraft in a three-body system is approximated using the CR3BP. This dynamical model assumes that two primary bodies gravitationally interact with a spacecraft [14]. The gravity field of each primary body, P_1 and P_2, is modeled as spherically symmetric, with constant masses [14]. However, the spacecraft is assumed to possess a negligibly small mass in comparison [14]. To support the construction of an autonomous dynamical model, the paths followed by the two primaries are assumed to be circular [14].

The CR3BP is often formulated using nondimensional coordinates. Length, mass, and time quantities are normalized to produce a distance between the two primaries, total system mass, and primary system mean motion all equal to unity [14]. In the Earth-Moon CR3BP, the length and time are normalized by $l^* = 384,400$ km and $t^* \approx 3.751903 \times 10^5$ sec, respectively. However, in the Sun-Earth CR3BP, $l^* = 1.495979 \times 10^8$ km and $t^* = 5.022635 \times 10^6$ sec [15].

A P_1-P_2 rotating frame is defined using the locations of the two primary bodies. The origin is selected as their barycenter whereas the axes $\hat{x}\hat{y}\hat{z}$ are defined as follows [14]: $\hat{x}$ is directed from the center of the larger primary to the center of the smaller primary; $\hat{z}$ is aligned with the orbital angular momentum vector of the primaries; and $\hat{y}$ completes the right-handed, orthogonal triad. With these definitions, the nondimensional state vector of the spacecraft is defined in the rotating frame as $\boldsymbol{x} = [\boldsymbol{r}^T, \boldsymbol{v}^T]^T$ where $\boldsymbol{r} = [x, y, z]^T$ and $\boldsymbol{v} = [\dot{x}, \dot{y}, \dot{z}]^T$; the dot notation indicates a time derivative with respect to an observer in the rotating frame.

The orientation of the rotating frame is often described relative to a general inertial frame. The axes of the inertial frame are labeled as $\hat{X}\hat{Y}\hat{Z}$. In addition, $\hat{Z} = \hat{z}$ whereas the angle between each of the $\hat{x}$ and $\hat{X}$ axes and the $\hat{y}$ and $\hat{Y}$ axes is equal to $\theta = nt$ where $n = 1$ is the nondimensional mean motion of the primary system and t is nondimensional time. The origin of the inertial frame may be selected as desired, e.g., at the barycenter or one of the primaries. With these definitions, the nondimensional state vector of the spacecraft is defined in the inertial frame as $\boldsymbol{X} = [\boldsymbol{R}^T, \boldsymbol{V}^T]^T$ where $\boldsymbol{R} = [X, Y, Z]^T$ and $\boldsymbol{V} = [X', Y', Z']^T$; the prime notation indicates a time derivative with respect to an observer in the inertial frame.

A state vector can be transformed between the rotating and inertial frames. The rotation matrices from the inertial frame to the rotating frame $[{}^R\boldsymbol{C}^I]$ and vice versa are defined as [16]

$$[{}^R\boldsymbol{C}^I] = \begin{bmatrix} \cos(\theta) & \sin(\theta) & 0 \\ -\sin(\theta) & \cos(\theta) & 0 \\ 0 & 0 & 1 \end{bmatrix} \qquad [{}^I\boldsymbol{C}^R] = \begin{bmatrix} \cos(\theta) & -\sin(\theta) & 0 \\ \sin(\theta) & \cos(\theta) & 0 \\ 0 & 0 & 1 \end{bmatrix} \tag{1}$$

where the I and R superscripts indicate the inertial and rotating frames, respectively. The time derivatives of these rotation matrices are calculated as

$$[{}^R\dot{\boldsymbol{C}}^I] = \dot{\theta} \begin{bmatrix} -\sin(\theta) & \cos(\theta) & 0 \\ -\cos(\theta) & -\sin(\theta) & 0 \\ 0 & 0 & 0 \end{bmatrix} \qquad [{}^I\dot{\boldsymbol{C}}^R] = \dot{\theta} \begin{bmatrix} -\sin(\theta) & -\cos(\theta) & 0 \\ \cos(\theta) & -\sin(\theta) & 0 \\ 0 & 0 & 0 \end{bmatrix} \tag{2}$$

Then, the position and velocity vectors are transformed from the rotating frame to the inertial frame, without a change of origin, as [16]

$$\boldsymbol{R} = [{}^I\dot{\boldsymbol{C}}^R]\boldsymbol{r} \qquad \boldsymbol{V} = [{}^I\boldsymbol{C}^R]\boldsymbol{v} + [{}^I\dot{\boldsymbol{C}}^R]\boldsymbol{r} \tag{3}$$

When shifting the origin of the inertial frame to a primary body, as opposed to the system barycenter, a translation is applied to only $\boldsymbol{r}$ prior to this transformation [16].

The equations of motion for the CR3BP are written in nondimensional form in the rotating frame. These second-order differential equations are equal to

$$\ddot{x} - 2\dot{y} = \frac{\partial U^*}{\partial x}, \qquad \ddot{y} + 2\dot{x} = \frac{\partial U^*}{\partial y}, \qquad \ddot{z} = \frac{\partial U^*}{\partial z} \tag{4}$$

where the pseudopotential function is defined as

$$U^* = \frac{x^2 + y^2}{2} + \frac{1 - \mu}{\rho_1} + \frac{\mu}{\rho_2} \tag{5}$$

and $\rho_1 = \sqrt{(x + \mu)^2 + y^2 + z^2}$, and $\rho_2 = \sqrt{(x - 1 + \mu)^2 + y^2 + z^2}$ [14]. Furthermore, μ is the mass ratio, equal to $1.215058535056245 \times 10^{-2}$ in the Earth-Moon CR3BP and $3.003480594542193 \times 10^{-6}$ in the Sun-Earth CR3BP [15]. An integral of motion exists in the rotating frame and is equal to $C_J = 2U^* - \dot{x}^2 - \dot{y}^2 - \dot{z}^2$ [14]. This quantity is labeled the Jacobi constant.

Patched Circular Restricted Three-Body Problems

The patched circular restricted three-body problem offers a low-fidelity approximation of the dynamical environment when three primary bodies exert a substantial gravitational force on the spacecraft [16]. Two CR3BPs are defined, with a common primary or barycenter of two primaries, to govern the dynamics in distinct regions. In this paper, the Earth-Moon and Sun-Earth CR3BP are employed, with the Earth serving as the larger primary in the Earth-Moon CR3BP and the smaller primary in the Sun-Earth CR3BP. Furthermore, for this proof of concept, the Earth-Moon and Sun-Earth planes are assumed to be coplanar due to the approximately 5° average angle between these planes; however, future work will eliminate this assumption. Solutions are connected between the Earth-Moon CR3BP and the Sun-Earth CR3BP only after the spacecraft reaches a nondimensional distance from the Earth equal to 1.4 in the Earth-Moon system.

To study the connectivity between trajectories generated in each of the Earth-Moon and Sun-Earth CR3BP, a spacecraft state vector must be transformed between distinct rotating frames and normalization schemes. Specifically, the nondimensional position and velocity vectors of the spacecraft in the Earth-Moon rotating frame, labeled as $\boldsymbol{r}_{EMB,sc}^{EM}$ and $\boldsymbol{v}_{EMB,sc}^{EM}$, are transformed to the Sun-Earth rotating frame, labeled as $\boldsymbol{r}_{SEB,sc}^{SE}$ and $\boldsymbol{v}_{SEB,sc}^{SE}$. In these vector labels, the superscripts 'EM' and 'SE' indicate the two primaries used to define the rotating frame and normalized: 'E' is the Earth, 'M' is the Moon, and 'S' is the Sun. The subscripts, however, identify the basepoint and target of the vector: 'EMB' is the Earth-Moon barycenter, 'SEB' is the Sun-Earth barycenter, and 'sc' is the spacecraft. At a given epoch t, this transformation consists of the following steps [16]:

1. Translate $\boldsymbol{r}_{EMB,sc}^{EM}$ from using an origin at the barycenter of the Earth-Moon system to the Earth by adding μ to the x-component, producing $\boldsymbol{r}_{E,sc}^{EM}$. The velocity vectors are unchanged, i.e., $\boldsymbol{v}_{E,sc}^{EM} = \boldsymbol{v}_{EMB,sc}^{EM}$ as the Earth is fixed in the rotating frame.
2. Transform $\boldsymbol{r}_{E,sc}^{EM}$ and $\boldsymbol{v}_{E,sc}^{EM}$ from the Earth-Moon rotating frame to the inertial frame centered at the Earth using Equation 3 to produce $\boldsymbol{R}_{E,sc}^{EM}$ and $\boldsymbol{V}_{E,sc}^{EM}$
3. Dimensionalize the position and velocity vectors in the inertial frame as well as the time using the characteristic quantities from the Earth-Moon CR3BP.
4. Nondimensionalize the position and velocity vectors in the inertial frame as well as the time using the characteristic quantities from the Sun-Earth CR3BP.
5. Transform $\boldsymbol{R}_{E,sc}^{SE}$ and $\boldsymbol{V}_{E,sc}^{SE}$ from the inertial frame centered at the Earth to the Sun-Earth rotating frame by substituting $[{}^{R}\boldsymbol{C}^{I}]$ into Equation 3 to produce $\boldsymbol{r}_{E,sc}^{SE}$ and $\boldsymbol{v}_{E,sc}^{SE}$.
6. Translate the position vector from using an origin at the Earth to the barycenter of the Sun-Earth system, by subtracting $1-\mu$ from the x-component to produce $\boldsymbol{r}_{SEB,sc}^{SE}$ and $\boldsymbol{v}_{SEB,sc}^{SE}$.

This transformation is influenced by the relative angle between the $\hat{x}$ axes in each of the Earth-Moon and Sun-Earth rotating frames, which is periodic over an interval labeled the synodic period and equal to 29.487 days when calculated using the characteristic quantities in this paper.

Curvature

Differential geometry is useful in studying curved paths, such as the solutions to a nonlinear, continuous time-system. A trajectory that is generated from a specified initial state vector over a time interval $t \in [t_0, t_f]$ traverses a distance equal to the arclength s that is calculated as [17]

$$s = \int_{t_0}^{t_f} ds = \int_{t_0}^{t_f} \sqrt{\dot{x}^2 + \dot{y}^2 + \dot{z}^2} dt \tag{6}$$

Furthermore, the curvature $\kappa(t)$ at a single state along the trajectory captures the deviation from a straight line in the osculating plane [18]. The unsigned curvature is calculated as

$$\kappa(t) = \frac{||\dot{\boldsymbol{r}}(t) \times \ddot{\boldsymbol{r}}(t)||}{||\dot{\boldsymbol{r}}(t)||^3} \tag{7}$$

where $\dot{\boldsymbol{r}} = \boldsymbol{v}$ is the velocity vector and $\ddot{\boldsymbol{r}} = [\ddot{x}, \ddot{y}, \ddot{z}]^T$ is the acceleration vector [18]. This expression possesses a singularity when the speed equals zero.

Density-Based Clustering

Clustering algorithms focus on discovering groupings formed by members of a dataset in a specified feature vector space [19]. Of the various approaches in the literature, density-based clustering algorithms construct clusters as members of the dataset that exist in regions of sufficiently high density. The current procedure for extracting motion primitives from trajectories generated in the CR3BP relies on the use of the following two density-based clustering algorithms [13]: Density-Based Spatial Clustering of Applications with Noise (DBSCAN), developed by Ester et al. [20]; and Hierarchical Density-Based Spatial Clustering of Applications with Noise (HDBSCAN), developed by Campello, Moulavi, and Sander [21].

DBSCAN discovers clusters as members that exist in high-density local neighborhoods of other members. This clustering algorithm relies on the definition of an m_{pts}-neighborhood as the local neighborhood of a current member that encompasses m_{pts} members in the selected feature vector space [20]. A core point is a member of a dataset with an m_{pts}-neighborhood that possesses a radius that is less than or equal to a specified value ϵ. A border point lies in the m_{pts}-neighborhood of a core point but its own m_{pts}-neighborhood possesses a radius that is larger than ϵ. A noise point does not exist in the m_{pts}-neighborhood of any core points. Using these definitions, a cluster is formed by 1) core points that lie within the ϵ-sized neighborhood of other core points and 2) their associated border points [20]. Thus, DBSCAN uniquely assigns each member to either a specific cluster or as noise. This algorithm is implemented using the *dbscan* function in MATLAB [22].

HDBSCAN extends DBSCAN by removing the dependence on a specified value of ϵ. To achieve this goal, the core distance of each member of the dataset is defined as the radius of its m_{pts}-neighborhood. This information is used to calculate a mutual reachability distance between each pair of points that further separates members that exist in low-density regions. This quantity is defined between the ith and jth members of the dataset as

$$d_{reach}(\boldsymbol{f}_i, \boldsymbol{f}_j) = \max(d_{core}(\boldsymbol{f}_i), d_{core}(\boldsymbol{f}_j), d(\boldsymbol{f}_i, \boldsymbol{f}_j)) \tag{8}$$

where $d(\boldsymbol{f}_i, \boldsymbol{f}_j)$ is the distance between their feature vectors, calculated using a specified distance measure [21]. HDBSCAN uses these distances to define the edge weights of a graph where each node corresponds to a member of the dataset [21]. A minimum spanning tree of this graph is then used to generate a hierarchy of all possible clustering results as a function of the mutual reachability distance. Clusters are selected from this hierarchy by locating grouping that maximize the stability of the result, assessed using an excess of mass definition [21]. Modifications to this cluster selection process include applying a minimum threshold ϵ_{merge} to the splitting of members into multiple clusters, as presented by Malzer and Baum [23]. Through this procedure, HDBSCAN uniquely assigns each member to either a specific cluster or as noise. Due to the use of a cluster hierarchy, irregularly shaped clusters can be extracted with distinct densities. This algorithm is implemented using the *hdbscan* library in Python [24].

TECHNICAL APPROACH

A motion primitive approach is used to generate initial guesses for planar trajectories in the patched Earth-Moon and Sun-Earth CR3BP. The most recent version of the primitive extraction process, presented by Gillespie, Miceli, and Bosanac [13], is used to form a motion primitive library. These primitives summarize arcs along the hyperbolic invariant manifolds of selected L_1 and L_2 Lyapunov orbits in each of the Earth-Moon and Sun-Earth planar CR3BP. Then, the recently updated version of this primitive-based trajectory design framework, developed by Miceli and Bosanac [12], is employed. Accordingly, a brief overview of this existing process is presented in this section; more details appear in each of the original papers. Furthermore, minor modifications are presented in this paper to accommodate the use of primitives generated in two distinct CR3BPs and a time-dependent assessment of their sequential composability.

Step 1: Generate Motion Primitive Library

Motion primitives are used to summarize arcs from stable and unstable manifolds of selected periodic orbits [13]. First, each periodic orbit is discretized into 500 states, equally spaced in arclength along the periodic orbit. Then, these states are perturbed along the planar stable and unstable modes of the periodic orbit, calculated from the monodromy matrix [16]. Each state that lies in the stable or unstable eigenspace is then propagated backward or forward in time, respectively for a duration that is equal to $\Delta t_{prop} = \Delta t_{pertdoub} + \Delta t_{des}$ [13]. In this expression, $\Delta t_{pertdoub}$ is the perturbation doubling time [25] whereas Δt_{des} is a specified, desired duration; Δt_{des} is selected as 3 months in the Earth-Moon system and 12 months in the Sun-Earth system. However, propagation terminates early if the spacecraft impacts a spherical approximation of the Sun, Earth, or Moon; their radii are equal to $695,700$ km, $6,378.137$ km, and $1,738$ km, respectively [26].

Arcs that are summarized using motion primitives are sampled from the hyperbolic invariant manifolds in a geometry-based manner [13]. As each trajectory is generated to lie in the stable or unstable manifold, the maxima in curvature are located [13]. These states correspond to geometrically meaningful locations along a trajectory, where the shape is rapidly changing. For trajectories that possess at least three curvature maxima, each arc begins at either a maximum in curvature or the initial condition [13]. Then, the arc is defined to span four additional maxima in curvature [13]. However, if the trajectory impacts the Earth or Moon, the trajectory ends at the termination condition. If a trajectory possesses fewer than three curvature maxima, the window used to define the arc is shortened accordingly. Through this approach, every arc begins at a consistently defined location and overlaps with the previous arc, if one exists.

Each continuous arc is discretized in a geometry-based manner to produce a sequence of states [13]. First, the arc is coarsely sampled at the initial state, intermediate maxima in curvature, and the final state; this first step produces up to five samples. Between subsequent coarse samples, two additional samples are equally distributed in the arclength along that segment [13]. Accordingly, a trajectory with three intermediate maxima between the initial and final states is sampled using 13 geometrically distributed states.

The sampled states are used to construct two feature vectors that capture the geometry of the trajectory in the rotating frame used in the CR3BP when generating the path [27]. First, a shape-based feature vector is defined as

$$\boldsymbol{f}_s = [\hat{\boldsymbol{v}}_1, \hat{\boldsymbol{v}}_2, ..., \hat{\boldsymbol{v}}_n]^T \tag{9}$$

where n is the number of sampled states and $\hat{\boldsymbol{v}}_i$ is the velocity unit vector at the ith sample in the

rotating frame. In addition, a position-based feature vector is defined using the position vectors in the rotating frame at each of the samples as

$$\boldsymbol{f}_p = [\boldsymbol{r}_1, \boldsymbol{r}_2, ..., \boldsymbol{r}_n]^T \tag{10}$$

Each feature vector is $3n$-dimensional.

Arcs extracted from the same stable or unstable half-manifold and sampled using the same number of states are coarsely clustered in the shape-based feature vector space, calculated over their entire duration, using HDBSCAN [13, 27]. At this step, $m_{pts} = 4$, $m_{minclust} = 5$, and $\epsilon_{merge} = 2\sin(5^\circ/2)$ [27]. Repeating this process for trajectories described by a distinct number of sampled states produces a set of coarse clusters $\mathcal{C}$ and noise. Any arcs labeled as noise are discarded from further consideration.

Arcs in each coarse group are input to a cluster refinement process originally developed by Bosanac [13, 27]. For each coarse group, the ith sampled state along each arc is used to calculate two three-dimensional feature vectors, $\boldsymbol{f}_s$ and $\boldsymbol{f}_p$. DBSCAN is used to independently cluster the sampled states in each of these two feature vector spaces, producing two clustering results. At this step, $m_{pts} = 4$ and $\epsilon = (m_{pts}+1)\max(\max(e_{med}, e_{maxk}), \epsilon_{thresh})$, where e_{med} is the median distance from each member to its nearest neighbor, e_{maxk} is the $m_{minclust}$-largest distance from each member to its nearest neighbor and ϵ_{thresh} is a specified threshold; in $\boldsymbol{f}_s$, $\epsilon_{threshold} = 2\sin(5^\circ/2)$ whereas in $\boldsymbol{f}_p$, $\epsilon_{threshold} = 10^{-3}$ in the Earth-Moon system and $\epsilon_{threshold} = 10^{-4}$ in the Sun-Earth system. This process is repeated across all n samples to produce $2n$ clustering results. Any trajectories that are consistently clustered together and possess at least $m_{minclust} = 5$ members form a refined cluster. The result of this step is a set of clusters $\mathcal{R}$ and noise. Any arcs labeled as noise are discarded from further consideration.

Each cluster is used to generate a motion primitive and its region of existence [13, 28]. The motion primitive is extracted as the medoid of the cluster in the position-based feature vector space, equal to the trajectory that follows the most similar path in the configuration space to all other trajectories. The region of existence is then the volume of the phase space spanned by all members of the cluster. Similar to the approach used by Smith and Bosanac [10] as well as Miceli and Bosanac [12], this region of existence is approximated using up to 40 trajectories that are equally distributed across the associated cluster. If a global cluster is composed of more than 40 members, a subset of 20 representative trajectories are identified by applying k-medoids clustering [29] in the position-based feature vector space of the entire trajectory using Matlab's built-in function [22].

The clusters that are localized to each half-manifold are aggregated to produce a smaller set of global clusters. First, the motion primitive of each cluster is compared to the primitives of all other clusters that are generated to approach or depart the same periodic orbit or a neighboring periodic orbit. Then, the nearest neighboring representatives in each of the position and velocity feature vector spaces are identified. Each pair of local clusters is then input to the cluster refinement process. If any members are grouped together, the local clusters are merged. Each global cluster contains one or more merged local clusters. Upon merging, the motion primitive and region of existence are updated.

This procedure is used to generate motion primitives that summarize arcs from the stable and unstable manifolds of selected L_1 and L_2 Lyapunov orbits in the Earth-Moon and Sun-Earth CR3BP. Selected motion primitives, generated in the Earth-Moon CR3BP and Sun-Earth CR3BP are plotted in Figures 1 and 2, respectively, to summarize groups of geometrically similar arcs that approach or

depart a) an L_1 Lyapunov orbit or b) an L_2 Lyapunov orbit. In these figures, the motion primitive is depicted with a thick blue curve whereas representative members of each cluster are plotted with thin blue curves. The initial state along each trajectory is indicated by a blue circle marker. Finally, the primaries are depicted with gray circle markers whereas L_1 and L_2 are plotted using gray diamonds. Within each subfigure, the motion primitive summarizes a set of geometrically similar trajectories. Furthermore, distinct motion primitives capture distinct geometries. For each of these four cases, the selected orbits as well as the number of clusters and assigned arcs are summarized in Table 1.

Step 2: Construct Motion Primitive Graph

A high-level, motion primitive graph is constructed to summarize the sequential composability of motion primitives in the library. Similar to the formulation presented by Miceli and Bosanac [12], nodes are defined as segments of motion primitives whereas directed edges are added between nodes where the associated segments exist sufficiently nearby in the phase space. These edges are then weighted to convey the ease of traversability, defined as a function of the change in velocity. However, this graph is modified to accommodate the use of primitives from two distinct dynamical models and to slightly increase the fidelity of the sequential composability assessment.

Nodes are defined as segments of each primitive and its region of existence [12]. Recall that each trajectory that lies within the region of existence of a motion primitive is already sampled geometrically as described in the previous subsection. Thus, the segments of all members of the region of existence between the ith and $(i+1)$th sampled states are represented by the ith node associated with a single primitive. Primitives in the generated library are described by up to 13 sampled states, including the initial and final states, that segment the trajectories into up to 12 sections. Therefore, each primitive contributes up to 12 nodes to the graph. Furthermore, a motion primitive graph that is constructed using N motion primitives possesses up to $12N$ nodes, before the inclusion of any nodes representing additional boundary conditions.

Directed edges are added between sequential nodes sampled from the same primitive and its region of existence [12]. A directed edge with a zero edge weight is added from the node representing the ith segment to the node of the $(i+1)$th segment along a single primitive, for $i < N_s$ where

	Earth-Moon L_1 Lyapunov	Earth-Moon L_2 Lyapunov	Sun-Earth L_1 Lyapunov	Sun-Earth L_2 Lyapunov
C_J	[3.003998, 3.188089]	[3.006767, 3.172112]	[3.0007867, 3.0008907]	[3.0007891, 3.0008867]
Period (days)	[11.692, 18.480]	[14.649, 19.203]	[175.067, 179.701]	[177.562, 181.730]
Number of clustered trajectories	70,836	24,945	5,999	5,345
Number of motion primitives	5,452	3,482	628	607

Table 1. Summary of motion primitives used to summarize arcs that approach or depart selected libration point orbits in the Earth-Moon or Sun-Earth CR3BP

.

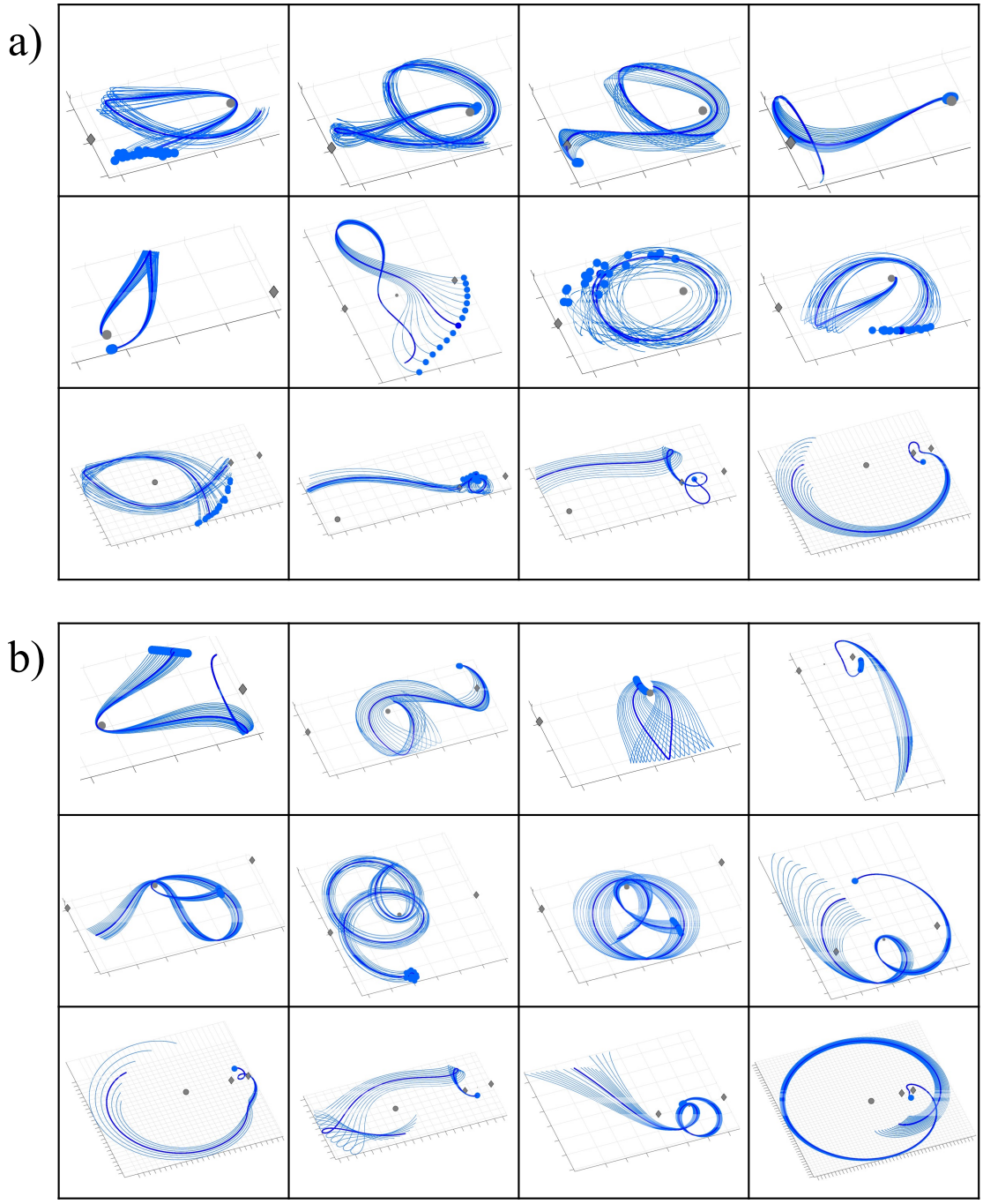

Figure 1. Selected motion primitives generated in the Earth-Moon CR3BP to approach or depart a) an L_1 Lyapunov orbit or b) an L_2 Lyapunov orbit.

N_s is the number of segments [12]. This edge encodes natural traversal of the primitive or any geometrically similar trajectory.

Using the procedure presented by Miceli and Bosanac [12] as a foundation, the region of existence associated with each primitive is coarsely approximated as a collection of circular neighborhoods

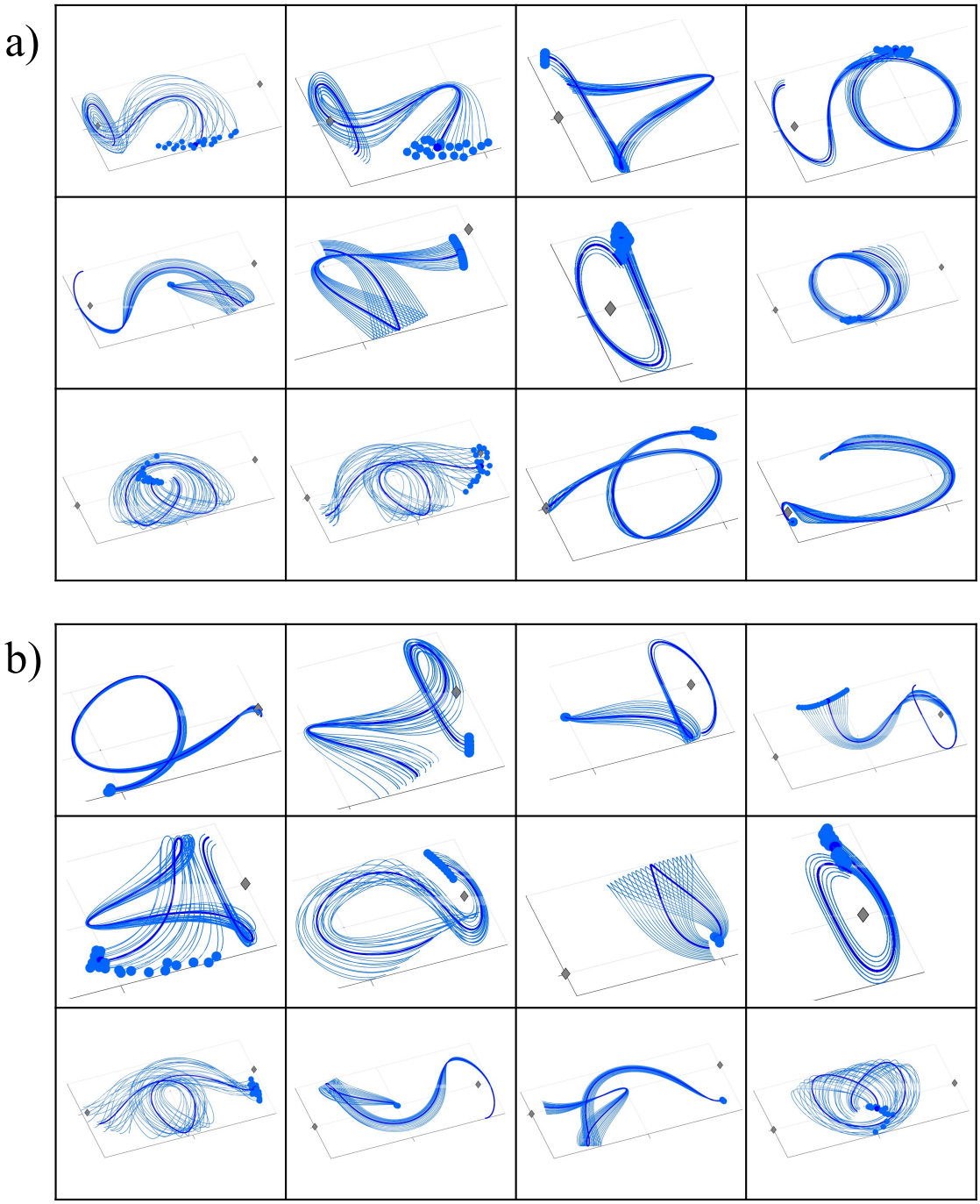

Figure 2. Selected motion primitives generated in the Sun-Earth CR3BP to approach or depart a) an L_1 Lyapunov orbit or b) an L_2 Lyapunov orbit.

around each sampled state. The representative trajectories that span the global cluster associated with a primitive are then further discretized to place up to 4 additional samples that are equally spaced in arclength along each segment, along with the initial state; this additional discretization step slightly increases the fidelity of the sequential composability assessment presented by Miceli

and Bosanac [12]. Then, neighborhoods are constructed around each sampled state in the configuration space. For the kth sampled state within the ith segment of any trajectory in the cluster, the neighborhood radius in the configuration space is approximated as the maximum of 1) the mean distance to the 2nd-nearest neighboring position vector along any other trajectories or 2) a predefined threshold, calculated as 5×10^{-3} in the Earth-Moon CR3BP or 5×10^{-4} in the Sun-Earth CR3BP. This slight modification to the definition presented by Miceli and Bosanac [12] supplies a larger neighborhood radius while reducing the bias of low mean distances between members of tightly-packed clusters. This process is repeated for all segments, coarsely approximating each region of existence via sets of circles.

Bidirectional edges are added between the nodes associated with segments of primitives within the same system if they are sequentially composable [12]. If these coarse approximations of the regions of existence of primitives 1 and 2 overlap in the configuration space at their ith and kth segments, respectively, with a change in the velocity direction that is less than $45°$, they are considered sequentially composable [12]. In this case, a bidirectional edge is added between the nodes representing the ith segment along primitive 1 and the kth segment along primitive 2. This edge is weighted by the following scalar quantity, also used by Bodin, Bosanac, and Gillespie [30]:

$$w_{1,i,2,k} = \frac{||\boldsymbol{v}_{1,l,i} - \boldsymbol{v}_{2,m,k}||}{||\boldsymbol{v}_{1,l,i}|| + ||\boldsymbol{v}_{2,m,k}||)} \tag{11}$$

where the subscripts in variables such as $\boldsymbol{v}_{1,l,i}$ indicate that the velocity vector is located along a state along segment i of trajectory l within the region of existence of primitive 1. Furthermore, trajectories l and m are selected from each region of existence to minimize the edge weight. The second term conveys the maneuver magnitude; as noted by Bruchko and Bosanac [31], normalizing this quantity by the sum of speeds reduces bias in the edge weights when the speed is high before or after the connection.

Directed edges are also added between primitives that are generated from different systems if they are sequentially composable. In this case, the sequential composability criteria are expanded to include the following conditions:

- The composable state along a motion primitive generated in the Earth-Moon CR3BP must reach a distance of at least $r_1 = 1.5$ from the Earth (the larger primary in this system).
- The motion primitive generated in the Sun-Earth CR3BP must pass closer to the Earth than any state along the motion primitive generated in the Earth-Moon CR3BP.
- The neighborhoods of the states along the primitive from the Earth-Moon CR3BP, after transformation to the Sun-Earth rotating frame, must overlap with the neighborhoods of the states along the primitive from the Sun-Earth CR3BP for any relative angle between the Earth-Moon and Sun-Earth rotating frames. This calculation is performed in the Sun-Earth rotating frame using quantities nondimensionalized in the Sun-Earth CR3BP.

Through this modification to the sequential composability assessment, the connection between the primitives generated in two different models must occur in the exterior region of the Earth-Moon system. Furthermore, the edge is directed from the node along a primitive generated in the Earth-Moon CR3BP to the node along a primitive generated in the Sun-Earth CR3BP. Accordingly, the trajectories are constrained to not return to the Earth-Moon system after departure in this preliminary implementation. The weight of each edge is then calculated using the same scalar quantity as in Equation 11, but using nondimensional coordinates in the Sun-Earth rotating frame. The edge weight is calculated using the lowest state discontinuity for any relative angle.

As presented by Miceli and Bosanac [12], path constraints can also be incorporated into the motion primitive graph. In this paper, the traversable nodes, i.e., those with edges that are connected to other nodes, are constrained to reflect the dominance of each CR3BP in distinct regions of the Sun-Earth-Moon system. First, a feasible segment along a primitive that is generated in the Sun-Earth CR3BP must possess at least one sampled trajectory that does not pass below a distance of 1.3 nondimensional units from the Earth when calculated using characteristic quantities from the Earth-Moon CR3BP. This constraint reflects that the Earth-Moon CR3BP is considered the dominant dynamical model below this distance, with some margin added. Similarly, a feasible segment along a primitive that is generated in the Earth-Moon CR3BP must possess at least one sampled trajectory that does not remain beyond a distance of 2.4 nondimensional units from the Earth when calculated using characteristic quantities from the Sun-Earth CR3BP; this value is selected using the Earth's sphere of influence. If all sampled trajectories along a segment of a region of existence associated with a primitive violate either criterion, the node is not connected to any other nodes in the graph.

The motion primitive library constructed in Step 1 is used to form a motion primitive graph with a higher-level structure that reflects the desired trajectory itineraries. This graph structure consists of two blocks, as depicted conceptually in Figure 3. The left block contains only nodes associated with segments along N primitives generated in the Earth-Moon CR3BP and the right block contains only nodes associated with segments along M primitives generated in the Sun-Earth CR3BP. In this figure, the label P_i next to a row of nodes, represented by circles, indicates that they represent segments associated with the ith primitive. The nodes within a single block can be connected via weighted, directed edges to nodes within the same block if they satisfy the path constraints and either 1) correspond to sequential segments of the same primitive as depicted by black arrows, or 2) correspond to sequentially composable segments along distinct primitives, as indicated by purple arrows. However, weighted, directed edges can only be added from nodes in the left block to nodes in the right block, as depicted by red arrows, if their segments are sequentially composable for any initial epoch in the Sun-Earth rotating frame. This motion primitive graph structure encodes an itinerary where the spacecraft travels within the Earth-Moon system and then departs to the exterior region to insert into a path that directly approaches an orbit in the Sun-Earth CR3BP. Although this graph definition supports the current proof of concept, ongoing work is focused on reducing the size and complexity of the motion primitive graph.

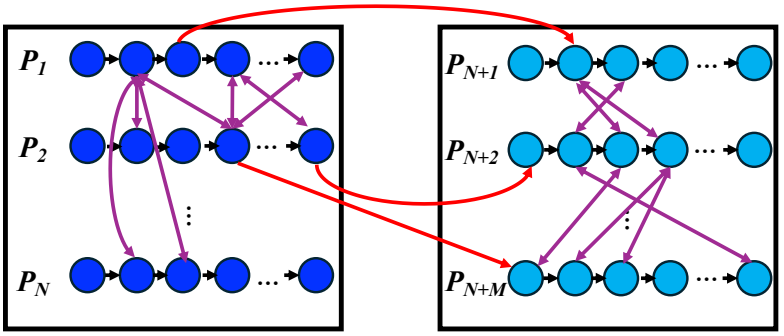

Figure 3. Conceptual depiction of high-level structure of motion primitive graph

Step 3: Search Motion Primitive Graph

The motion primitive graph is searched to produce paths, each composed of nodes and edges, that are transformed to primitive sequences. First, Dijkstra's algorithm is used to generate a single path through the graph. This solution is then converted to the associated primitive sequence, with each primitive sampled to retain only the segments associated with the nodes that appear in the sequence. In this paper, the initial epoch is assumed to be unconstrained; this assumption substantially reduces the complexity of the search process as edges between primitives from distinct dynamical models are fixed at each iteration of the graph search. Ongoing work includes incorporating a fixed initial epoch into the graph search process.

Dijkstra's algorithm is employed to generate a sequence of nodes and edges that connect a start node to an end node. This algorithm, developed by Edsger Dijkstra [32], begins by defining a priority queue that consists of the start node with a zero cost. Then, the lowest cost entry in the priority code produces a path from the start node, n_s. The final node along this path is designated as the current node, n_i. Each previously unvisited neighboring node is identified using the edges of the graph. The cumulative cost to reach neighbor n_{i+1} is then calculated as $g(n_s, n_{i+1}) = g(n_s, n_i) + g(n_i, n_{i+1})$ where $g(n_s, n_i)$ is the current cumulative cost from the start node n_s to node n_i. This neighboring node is also marked as having been visited. The cost and the path from the start node to the neighbor n_{i+1} are then added to the priority queue. This process is repeated for all neighbors of the current node. Then, the priority queue is sorted by the value of g and the lowest cost path is selected for further exploration from its last node. This process continues until the end node is reached or the priority queue is empty. If successful, the output of this process is the path that minimizes the cumulative edge weights.

To support exploring a tradespace, k solutions are generated. Following the work of Bruchko and Bosanac [31] and then Miceli and Bosanac [12], Yen's algorithm is used to compute these additional solutions. Yen's algorithm is a k-shortest paths algorithm that relies on the use of modified subgraphs to generate suboptimal solutions [33]. Once the first path has been computed via Dijkstra's algorithm, the edge between nodes n_i and n_{i+1} in the solution is removed from the graph to produce a subgraph. The portion of the path from the start node n_s to the current node n_i is labeled the spur path. Then, Dijkstra's algorithm is used to generate a path through the graph from node n_i to the end node n_e. This path is concatenated to the spur path. Then, the combined path is added to a list along with its total cost. This process is repeated for all edges between subsequent nodes along the most recently computed path, removing only one edge from the graph at each iteration. The next best path from those currently identified is used to repeat the process. However, at this step, if the current node is identified as n_i, all edges that connect n_i to any subsequent nodes along previously explored solutions are removed from the subgraph. This entire process is repeated until k solutions have been generated.

Step 4: Generate Initial Guess from Primitive Sequence

A primitive sequence computed in the previous step is used to generate an initial guess for a planar transfer between an L_1 Lyapunov orbit in the Earth-Moon CR3BP to a Sun-Earth L_2 Lyapunov orbit. This process follows the formulation developed by Miceli and Bosanac [12] that relies on constructing a localized graph. The result is a set of arcs, sampled from the region of existence of each primitive, that supplies a discontinuous initial guess for a transfer while retaining the geometry of the original primitive sequence. Although this paper does not correct or optimize these initial guesses, this step will be included in future work.

The localized graph defines the nodes as the traversed segments of the representative trajectories within the region of existence of each primitive in the sequence [12]. First, each of the representative trajectories spanning the region of existence of a primitive is segmented using the same procedure as described in Step 2. However, at this step, the segment of each trajectory between the ith and $(i+1)$th sampled states contributes a node to the graph. Accordingly, a region of existence that is coarsely represented by 20 trajectories that are each discretized into 12 segments would contribute 240 nodes if the entire primitive is traversed. However, if only segments 2 to 5 were traversed in the original primitive sequence generated in Step 3, this region of existence would contribute only 80 nodes. Thus, a primitive sequence composed of A primitives that are partially or fully traversed would be represented by a localized graph of up to $480A$ nodes.

Edges are added between the nodes of the localized graph in a manner that reflects the primitive sequence. First, directed, zero-weight edges are added between sequential segments along the same trajectory. Then, edges are added from the end of the last traversed segment of each trajectory associated with one primitive to the start of the traversed segment of every trajectory associated with the subsequent primitive, if their segments are sequentially composable. The edge between node i and node j is assigned the following edge weight:

$$w_{i,j} = ||\boldsymbol{r}_i - \boldsymbol{r}_j|| + 0.01\left(1 - \cos\left(\frac{\boldsymbol{v}_i \cdot \boldsymbol{v}_j}{||\boldsymbol{v}_i||||\boldsymbol{v}_j||}\right)\right) \tag{12}$$

when the position and velocity vectors are associated with the combination of discretely sampled states along each segment that minimize this edge weight. In this definition, the first term incentivizes reducing the position discontinuity during refinement whereas the second term includes, to a lesser extent, the change in the velocity direction through an impulsive maneuver. If the two nodes correspond to the segments of trajectories that are generated in distinct dynamical models, two modifications are employed: 1) the position and velocity vectors of the trajectory from the Earth-Moon CR3BP are transformed to the Sun-Earth rotating frame, and 2) the epoch that produces the lowest edge weight is used in this calculation.

The localized graph is searched using Dijsktra's algorithm to generate an initial guess. The search process produces a sequence of arcs along trajectories sampled from within the region of existence of the primitives in the identified sequence. These arcs form the initial guess for a trajectory.

RESULTS

A motion primitive graph is generated and searched to produce initial guesses from primitives associated with libration point orbits in the Earth-Moon CR3BP to primitives associated with libration point orbits in the Sun-Earth CR3BP. For computational efficiency in this proof of concept, this motion primitive graph is formed using 216 selected members of the motion primitive library. The resulting graph consists of 2,529 nodes and 315,683 edges. A few different initial and final primitives are selected to define the boundary conditions for the graph search.

Three examples of geometrically distinct initial guesses between various initial and final primitives are depicted in Figures 4-5. The lefthand side of each figure depicts part of the initial guess in the Earth-Moon rotating frame, zoomed into the vicinity of the Moon, whereas the righthand side of each figure depicts part of the initial guess in the Sun-Earth rotating frame. In this rightmost subfigure, the arcs generated in the Earth-Moon CR3BP are plotted in red whereas the arcs generated in the Sun-Earth CR3BP are plotted in blue. Across all subfigures, the start of each arc is indicated by a circle with the arrows indicating direction of motion and the Earth and Moon are indicated, but

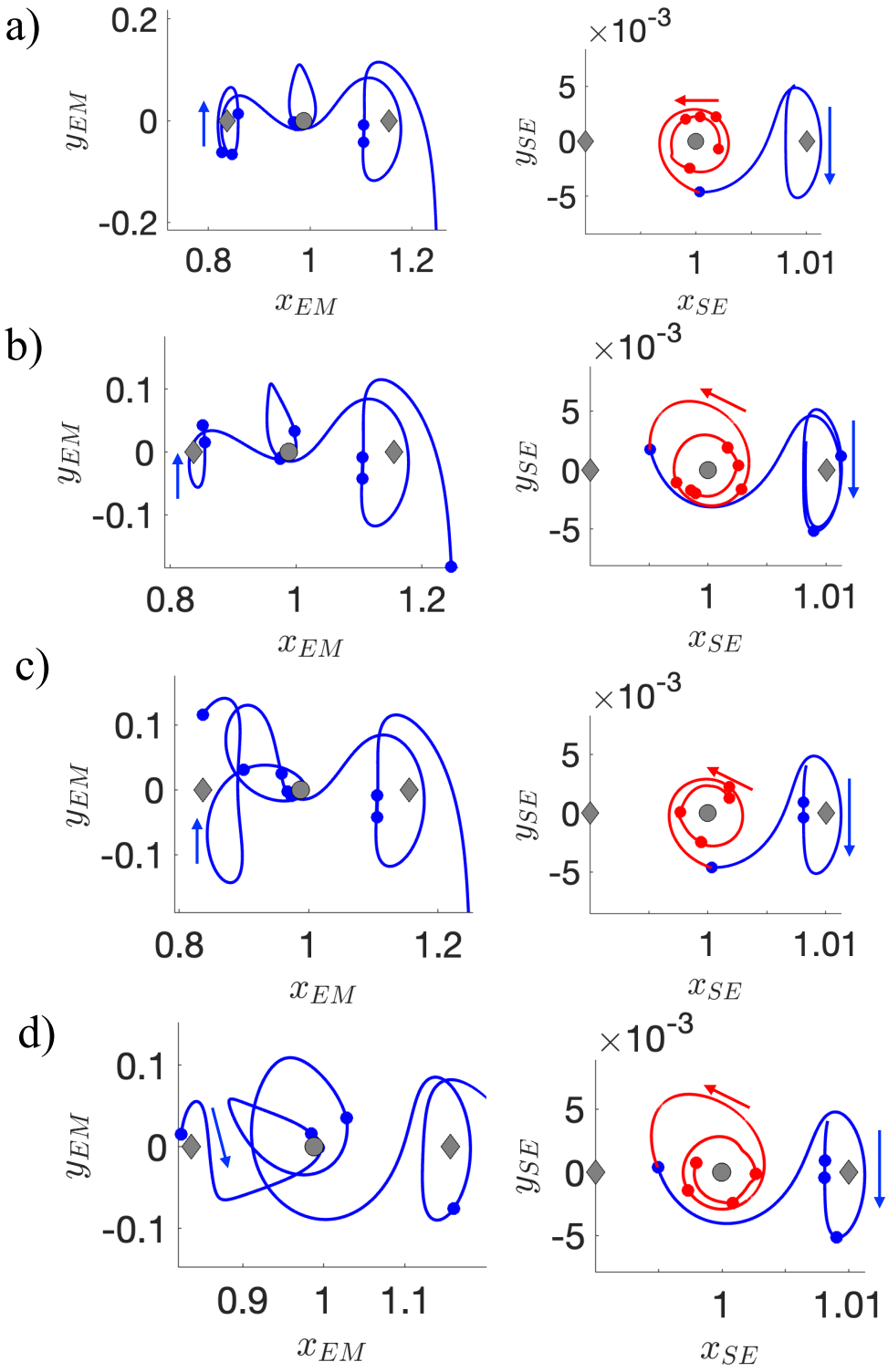

Figure 4. Examples of initial guesses for trajectories from an arc departing an Earth-Moon L_1 Lyapunov orbit to an arc approaching a Sun-Earth L_2 Lyapunov orbit.

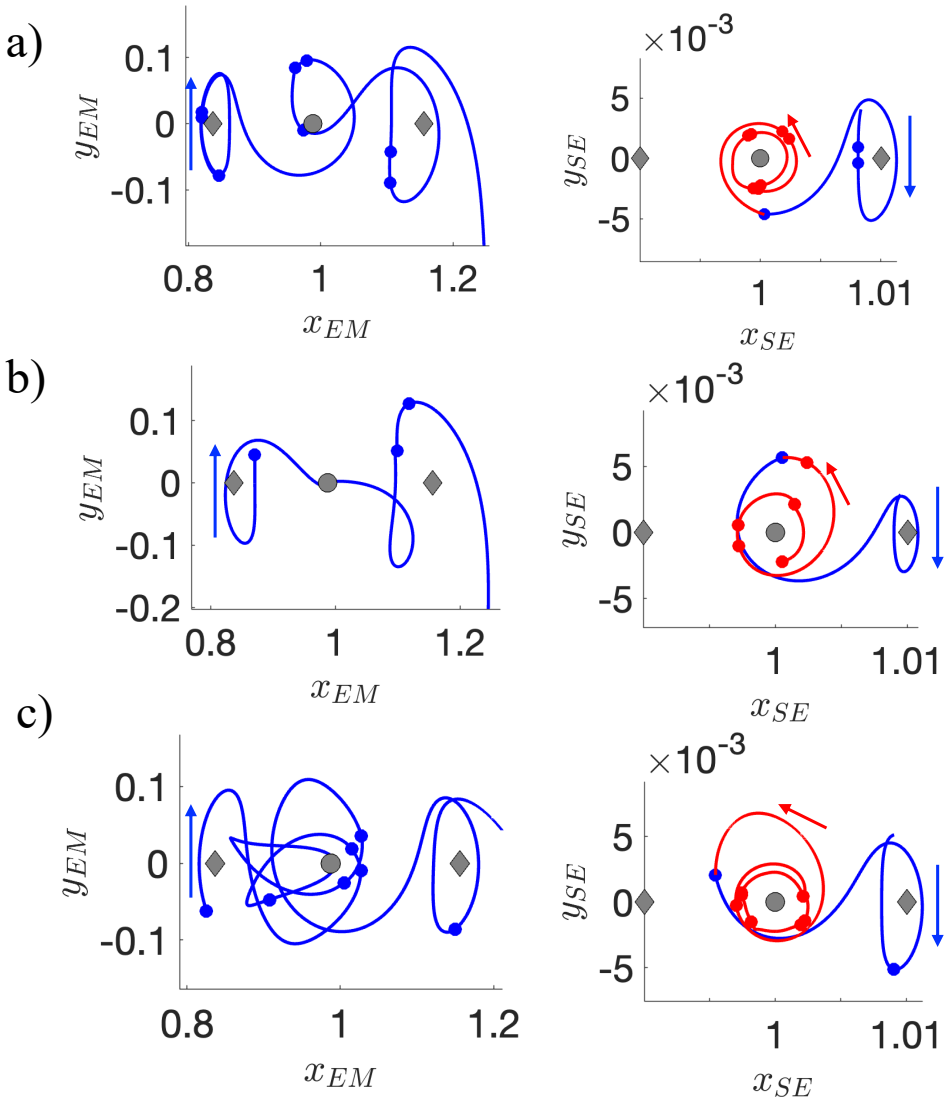

Figure 5. Examples of initial guesses for trajectories from an arc departing an Earth-Moon L_1 Lyapunov orbit to an arc approaching a Sun-Earth L_2 Lyapunov orbit.

not to scale. In these three examples, the transfers are geometrically distinct and visually appear to produce paths with relatively low position discontinuities. Analysis of the energy changes and required maneuver magnitudes is an avenue for future work. Furthermore, the inclusion of all members of the motion primitive library is expected to drastically expand the number of geometrically diverse initial guesses.

CONCLUSIONS

This paper leveraged a motion primitive approach to generate planar initial guesses for spacecraft trajectories from an Earth-Moon L_1 Lyapunov orbit to a Sun-Earth L_2 Lyapunov orbit. This paper leveraged an approach previously developed by Miceli and Bosanac [12], with minor modifications to incorporate the use of primitives from two different dynamical models. Ongoing work is focused

on generating a wider array of the initial guesses using the entire motion primitive library and correcting the initial guesses to produce continuous, maneuver-enabled transfers.

ACKNOWLEDGMENT

Part of this paper is based upon work supported by the Air Force Office of Scientific Research under award number FA9550-23-1-0235. Any opinions, findings, and conclusions or recommendations expressed in this material are those of the authors and do not necessarily reflect the views of the United States Air Force.

REFERENCES

[1] H. Willenberg, M. Fruhwirth, and S. Potter, "Site Selection and Deployment Scenarios for Servicing of Deep-Space Observatories," in *Proceedings, IEEE Aerospace Conference*, IEEE, 2002.

[2] C. Lillie, "On-Orbit Servicing for Future Space Observatories," in *Space 2005*, Long Beach, CA, Aug. 2005.

[3] B. Naasz, "Concepts for Servicing Habitable Worlds Observatory," in *Pioneering Sustainable Observatories, Summer 2024 Workshop Exploring Servicing Capabilities for the Habitable Worlds Observatory*, Presentation, 2024.

[4] R. Farquhar, D. Muhonen, and L. Church, "Trajectories and Orbital Maneuvers for the ISEE-3/1CE Comet Mission," in *AAS/AIAA Astrodynamics Conference*, Seattle, WA, 1984.

[5] K. Howell, B. Barden, and M. Lo, "Application of Dynamical Systems Theory to Trajectory Design for a Libration Point Mission," *The Journal of the Astronautical Sciences*, vol. 45, no. 2, pp. 161–178, 1997.

[6] D. Folta and C. Webster, "Transfer Trajectory Options for Servicing Sun-Earth-Moon Libration Point Missions," in *AAS/AIAA Space Flight Mechanics Meeting*, Ka'anapali, HI, 2019.

[7] J. Romero and K. Howell, "Transfers from Geosynchronous Transfer Orbits to Sun-Earth Libration Point Trajectories," *The Journal of the Astronautical Sciences*, vol. 69, pp. 251–283, 2022.

[8] A. Pascarella, R. Bommena, S. Eggl, and R. Woollands, "Mission Design for Space Telescope Servicing at Sun-Earth L2," *Acta Astronautica*, pp. 397–414, 2024.

[9] T. Smith and N. Bosanac, "Constructing Motion Primitive Sets to Summarize Periodic Orbit Families and Hyperbolic Invariant Manifolds in a Multi-Body Systems," *Celestial Mechanics and Dynamical Astronomy*, vol. 134, no. 7, 2022.

[10] T. Smith and N. Bosanac, "'Motion Primitive Approach to Spacecraft Trajectory Design in a Multi-Body System," *The Journal of the Astronautical Sciences*, vol. 70, no. 34, 2023.

[11] A. Wolek and C. Woolsey, "Model-Based Path Planning," in *Sensing and Control for Autonomous Vehicles: Application to Land, Water and Air Vehicles*. Berlin: Springer, 2017.

[12] G. Miceli and N. Bosanac, *Generating Trajectories for Neptunian System Exploration Using Motion Primitives*, Under review, 2025.

[13] G. Gillespie C. Miceli and N. Bosanac, "Summarizing Natural and Controlled Motion in Cislunar Space With Behavioral Motion Primitives," in *AAS/AIAA Space Flight Mechanics Meeting*, Kaua'i, HI, Jan. 2025.

[14] V. Szebehely, *Theory of Orbits: The Restricted Problem of Three Bodies*. London: Academic Press, 1967.

[15] W. Folkner, J. Williams, and D. Boggs, "The Planetary and Lunar Ephemeris DE 421," *The Interplanetary Network Progress Report*, vol. 42, no. 178, 2009.

[16] W. S. Koon, M. W. Lo, J. E. Marsden, and S. D. Ross, *Dynamical Systems, the Three Body Problem and Space Mission Design*. New York: Marsden Books, 2011.

[17] K. Wardle, *Differential Geometry*. Mineola, NY: Dover Publications, Inc., 2008.

[18] N. Patrikalakis, T. Maekawa, and W. Cho, *Shape Interrogation for Computer Aided Design and Manufacturing*. 2009.

[19] J. Han and M. Kamber, *Data Mining: Concepts and Techniques, 2nd ed.* New York, NY: Proquest EBook Central: Elsevier Science and Technology, 2006, ch. 7.

[20] M. Ester, H. Kriegel, J. Sander, and X. Xu, "A Density-Based Algorithm for Discovering Clusters in Large Spatial Databases with Noise," in *Proceedings of the Second International Conference on Knowledge Discovery and Data Mining*, AAAI Press, 1996.

[21] R. Campello, D. Moulavi, and J. Sander, "Density-Based Clustering Based on Hierarchical Density Estimates," in *Advances in Knowledge Discovery and Data Mining*, J. Pei, V. Tseng, L. Cao, H. Motoda, and G. Xu, Eds., Heidelberg: Springer, Berlin, 2013.

[22] The MathWorks Inc., *MATLAB version: 9.14 (R2023a)*, Natick, Massachusetts, United States, 2023. [Online]. Available: `https://www.mathworks.com`.

[23] C. Malzer and M. Baum, "A Hybrid Approach To Hierarchical Density-Based Cluster Selection," in *2020 IEEE International Conference on Multisensor Fusion and Integration for Intelligent Systems*, 2020, pp. 223–228.

[24] L. McInnes, J. Healy, and S. Astels, "hdbscan: Hierarchical Density Based Clustering," *Journal of Open Source Software*, vol. 2, no. 11, 2017.

[25] J. S. Parker and R. L. Anderson, *Low-Energy Lunar Trajectory Design*. Hoboken, New Jersey: John Wiley & Sons, 2014.

[26] NASA Goddard Space Flight Center, *General Mission Analysis Tool Version R2020a: Mathematical Specifications*, 2020.

[27] N. Bosanac, "Data-Driven Summary of Motion in an Ephemeris Model of Cislunar Space," in *AAS/AIAA Space Flight Mechanics Meeting*, Kaua'i, HI, Jan. 2025.

[28] N. Bosanac, "Data-Mining Approach to Poincaré Maps in Multi-Body Trajectory Design," *Journal of Guidance, Control, and Dynamics*, vol. 43, no. 6, 2020.

[29] L. Kaufman and P. Rousseeuw, "Finding Groups in Data," in John Wiley Sons, Inc., 1990, ch. Partitioning Around Medoids (Program PAM), doi:10.1002/9780470316801.ch2.

[30] A. Bodin, N. Bosanac, and C. Gillespie, "Long-Term Spacecraft Trajectory Prediction Using Behavioral Motion Primitives," in *AAS/AIAA Astrodynamics Specialist Conference*, Boston, MA, 2025.

[31] K. Bruchko and N. Bosanac, "Rapid Trajectory Design in Multi-Body Systems Using Sampling-Based Kinodynamic Planning," *The Journal of the Astronautical Sciences*, vol. 72, no. 33, 2025.

[32] E. Dijkstra, “A Note on Two Problems in Connexion with Graphs,” *Numerische Mathematik*, vol. 1, pp. 269–271, 1959, doi:10.1007/BF01386390.

[33] J. Yen, “Finding the k Shortest Loopless Paths in a Network,” *Management Science*, vol. 17, pp. 712–716, 1971.